A&A 402, 1103–1113 (2003)
DOI: 10.1051/0004-6361:20030221

Astronomy & Astrophysics

A comparison between the CaII(k_3), H_α, SOHO/MDI and radio-enhanced temperature regions of the Sun

A. Riehokainen[1], E. Valtaoja[1,2], and S. Pohjolainen[1]

[1] Tuorla Observatory, 21500 Piikkiö, Finland
[2] Metsähovi Radio Observatory, Helsinki Univ. of Technology, Espoo, Finland

Received 4 September 2002 / Accepted 21 January 2003

Abstract. We present a comparison of the enhanced temperature regions (ETRs) in the radio emission of the Sun with other manifestations of solar activity over 5 days. The radio observations at 87 GHz were observed with the Metsähovi Radio Telescope (Finland). We superposed the intensity contours of the full-disk radio maps on the Meudon spectroheliograph CaII(k_3) and H_α images of the Sun for comparisons between the radio and the optical positions and brightness characteristics of these active areas. A similar comparison to the SOHO satellite's Magnetic Doppler Imager magnetograms was also made. We concentrated on the high and low latitude weak radio ETRs with no discernible connections to sunspots. No distinction was made between radio ETRs inside and outside of coronal holes. A close connection between the radio and the optical activity was found. The average CaII(k_3)/ H_α brightness of the whole radio ETR is almost always above the disk average. The CaII(k_3), the H_α and the radio brightness inside individual ETRs are also correlated. We found that the radio maximum in general coincides either with the brightest CaII(k_3)/ H_α and strongest magnetic field structures within the ETR area, or with a density enhancement of the less bright CaII(k_3)/ H_α and less strong magnetic field structures. It is possible that these two cases result from different (unresolvable) fine structures of the radio ETRs. We suggest that the high and the low latitude weak ETRs may have several causes, which explains the lack of one-to-one correlations with other manifestations of solar activity.

Key words. Sun: radio radiation – Sun: faculae, plages – Sun: magnetic fields

1. Introduction

The enhanced temperature regions (ETRs in the following) in the radio emission at high solar latitudes in the polar coronal holes were discovered by Babin et al. (1976) and Efanov et al. (1980). This was surprising, because at almost all other wavelength coronal holes are seen as darker areas. Long-term observations of the ETRs with the Metsähovi radio telescope at frequencies of 37 GHz and 87 GHz have shown that their sizes can exceed several arcminutes. The typical temperature enhancements range from 200 K to 600 K. The typical lifetimes are of the order of a few hours, but some ETRs can last for several days (Riehokainen et al. 1998). The most likely radiation mechanism is thermal bremsstrahlung.

A number of papers by various authors have suggested that the ETRs could be connected with coronal hole brightenings depending on magnetic field configurations (Kosugi et al. 1986; Gopalswamy et al. 1999), polar plumes (Gopalswamy et al. 1992), microwave enhancements superposed on limb brightenings (Shibasaki et al. 1997), diffuse brightenings, bright points and polar plumes (Pohjolainen et al. 2000) and polar faculae groups (Riehokainen et al. 1998, 2001). No one-to-one correlation with coronal features has been found, and the nature of the polar radio brightenings is still unresolved. The high latitude ETRs are also important for the study of the polar component of the solar activity cycle. The polar ETR activity cycle seems to track the polar faculae cycle, both in antiphase with the sunspot cycle (Riehokainen et al. 1998; Gelfreikh et al. 2002a,b).

In our previous paper (Riehokainen et al. 2001) we showed that high-latitude ETRs are connected to some brightness structures. In many cases these structures look like cells. The boundaries of these cells were slightly brighter than the area inside, as seen in the SOHO satellite's Extreme ultraviolet Imaging Telescope (EIT) 171 Å images. Polar faculae groups are preferably situated at the cells' boundaries or inside the cells. The ETR maxima are located within these cells, and their boundaries generally coincide with the boundaries of the cells.

There are ETRs also at low solar latitudes. It is well known that the strongest of them are related to sunspots. Relatively weak ETRs, on the other hand, could be related to other manifestations of solar activity, such as faculae or plages. The equatorial coronal hole radio brightenings have been associated with the H_α intranetwork brightenings (Moran et al. 2001). In this study we investigate both high and low latitude weak ETRs, both inside and outside of coronal holes, with the aim

Send offprint requests to: A. Riehokainen,
e-mail: alrieho@astro.utu.fi

of finding if they are manifestations of the same processes. For comparison, we also include a few sunspot-related strong ETRs in our analysis.

It is well known that the radio emission at different wavelengths originates at different heights in the quiet solar atmosphere and depends on the temperature and the density of the charged particles. Using the Vernazza et al. (1981) atmospheric model, we can estimate that the radio emission at 3 mm, the wavelength used in this study, originates approximately at the same height and under the same temperature conditions as the emission in CaII(k_3) and H_α lines. Thus, a reasonable hypothesis, investigated in the present paper, is that some connection between the radio enhancements and the brightness enhancements in CaII(k_3) and H_α can be found. In addition, we also consider the distribution of magnetic field sources (at the photosphere level) inside the ETR areas, as mapped by the Michelson Doppler Imager (MDI) magnetograms of the SOHO satellite. Whatever the mechanisms generating the ETRs and the various brightness structures, it is likely that they are connected to, and governed by, the magnetic field structures of the Sun.

As previous investigations have shown, there are several manifestations of solar activity which can be responsible for the ETRs at both high and low solar latitudes. On the other hand, it is also possible that ETRs are complex phenomena that can have a number of different physical causes. Unfortunately, the Metsähovi radio telescope with one arcmin beam size cannot resolve the fine structure which we can see in the optical images. However, we can study what kind of surface configurations of the brightness structures preferentially correspond to the ETRs.

In our analysis we first define the intensity contours of the radio ETRs found in 87 GHz full disk solar maps. These are then superposed on the CaII(k_3), H_α and MDI maps for quantitative comparisons between radio and other wavelength data. Our main goals are to find out if the radio ETRs exhibit unusual characteristics also at other wavelengths, and if there are any differences between high and low latitude weak ETRs.

2. Observational data

Our starting point is data from the Metsähovi Radio Observatory (radio telescope with 13.7 m parabolic dish) at 87 GHz (3 mm). The spatial resolution at 87 GHz is 1 arcmin. The quiet Sun brightness temperature has been estimated to be around 7200 K (1.0 in normalized units). The resolution in brightness temperature is about 22 K. The details of the Metsähovi mapping method and error analysis for coordinate determination can be found in Pohjolainen et al. (2000).

All our radio data were obtained during 5 days; August 7 and 26, 1997, May 11 and 12, 1998, and August 22, 2000. The 1997 data were also used in our previous work (Riehokainen et al. 2001), but no quantitative analysis was attempted in that paper. For each day we selected one 87 GHz radio map (one example of a radio map used in this work is given in Fig. 1) for our analysis, the time as close as possible to the other wavelength data. For magnetic field data we used the full-disk

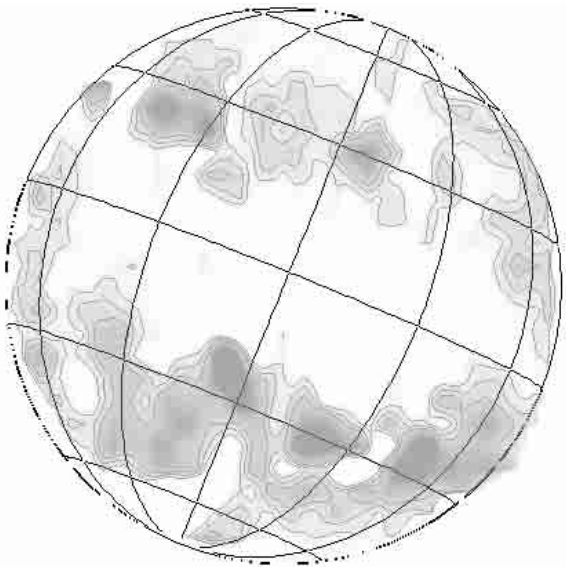

Fig. 1. Full disk 87 GHz image (or map) obtained at Metsähovi on May 12, 1998. The three lowest radio contours 0, 100, 200 K above the quiet Sun level (7200 K) are shown. Areas with larger enhancement are shown in gray scale only. The high latitude ETR close to the South Pole is shown in Fig. 4 also.

magnetograms recorded daily by the SOHO/MDI (Michelson Doppler Imager). For optical data we used the Meudon spectroheliograph full disk data from the Observatoire de Paris, Meudon: intensitygrams in H_α 6563 Å line and intensitygrams in CaII K 3934 Å line (center or k_3). In comparisons between the various wavelengths we have used nearly simultaneous observational data, the maximum time difference being about 30 min. For this reason we did not make corrections for the differential rotation.

3. Analysis of the observational data

We used the same procedure for the data analysis on each of the five days. First the quiet Sun level was defined for each radio map and a contour map of the radio intensity was constructed. Next we identified the regions with enhanced radio brightness and measured the maximal values of the temperature enhancements.

Each ETR was defined by a contour map (lines of equal brightness or temperature). Figure 2 shows schematically the characteristics that were used in this study. R is the position of the maximum of the ETR. The first contour is the quiet Sun level (T = 7200 K, or 1.0 in normalized units) or, in the case of adjacent ETRs, the borderline to the neighboring ETR. The other contours correspond to temperatures $T_i = 7200 + step * i$, where $i = 1, 2...n$ and $step$ is some constant value (usually around 20 K). Thus for each ETR we have a set of contours which we denote by $\{k_n\}$: k_1, k_2,...k_n, as shown in Fig. 2. Then we measured the area within each contour: $S_1, S_2...S_n$ (denoted by $\{S_n\}$). After that, we calculated the average radio brightness within each contour, $r_{\mathrm{av}1}, r_{\mathrm{av}2}...r_{\mathrm{av}n}$ (denoted by $\{r_{\mathrm{av}n}\}$).

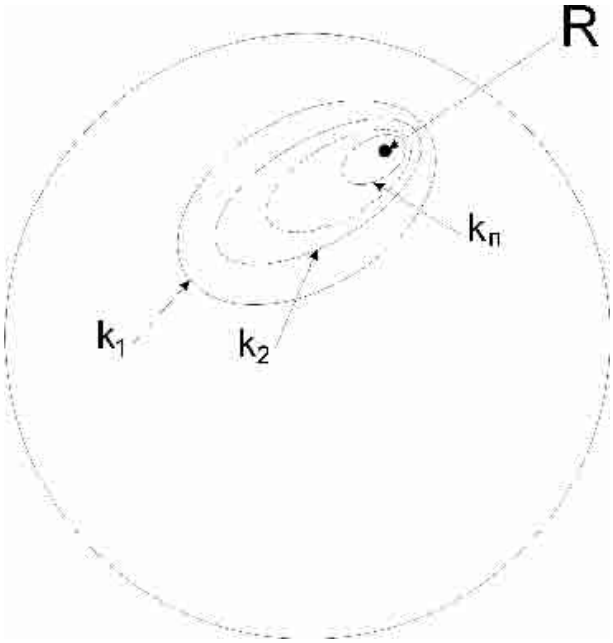

Fig. 2. The ETR maximum position R and the intensity contours $\{k_n\}$.

Thus, for each ETR we have the position of its center (latitude, longitude and r/R which is the relative distance from the center of the Sun), its size (in million parts of the solar hemisphere, msh), and its average radio brightness (in instrumental units) within each intensity contour.

As the next step, we superposed the ETR contours on the corresponding CaII(k_3) and H_α maps, and on the SOHO/MDI magnetograms, as shown in Fig. 4. Within each superposed radio contour, we calculated the average CaII(k_3) brightness: $Ca_{\rm av1}, Ca_{\rm av2}...Ca_{\rm avn}$ (denoted by $\{Ca_{\rm avn}\}$) and also found the maximal values for the brightness $\{Ca_{\max n}\}$ inside each contour. Similarly, for the H_α maps we determined $\{H_{\rm avn}\}$ and $\{H_{\max n}\}$ and for the magnetograms $\{m_{\rm avn}\}$ and $\{m_{\max n}\}$. We calculated separately both (the negative and the positive) maximal values of the magnetic field. (The areas within the contours were of course equal to $\{S_n\}$.)

In order to eliminate the limb darkening effect which is seen in the CaII(k_3) and H_α solar images, the measured values were corrected using the factor $1/f(r/R)$, where r/R is the relative distance from the solar center and $f(r/R)$ is a function obtained by polynomial fitting of the brightness distribution over the solar disk, defining the "quiet Sun level" for the corresponding image (cf. Fig. 3). We excluded regions close to the solar limb ($r/R > 0.9$) from our analysis, since they are very strongly affected by the artificial limb darkening.

One example of a real ETR superposed on the corresponding CaII(k_3), H_α images and magnetogram is presented in Fig. 4. The first white contour is the quiet Sun level, defining the outer limit of the ETR. The second white contour is close to the radio maximum level (intermediate contours have been omitted for clarity). The black circle (on the fragment of the SOHO/MDI magnetogram) shows the radio telescope beam size. On the left hand of the figure we show the measured relations between the average radio brightness and corresponding average and maximal values of CaII(k_3), H_α brightness and the magnetic field.

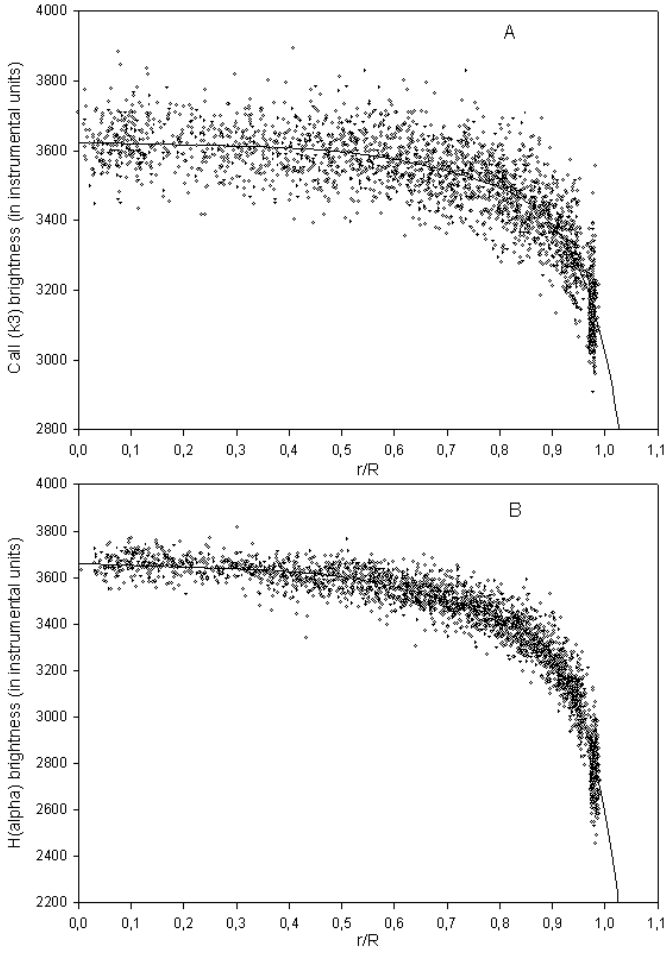

Fig. 3. An example of the brightness distributions over the solar disk, obtained on May 12, 1998. **A)**: corresponds to the CaII(k_3) solar image, **B)**: to the H_α solar image. r/R is the relative distance from the solar center, and each dot corresponds to one brightness measurement. The fitted functions $f(r/R)$ are shown by the solid curves.

In Fig. 5 we show a typical example of the relation between the average radio brightness and the average CaII(k_3) brightness with error bars for the region shown in Fig. 4. We note that the errors in average brightness determination are smaller than the variation from contour to contour.

4. Results

The total number of ETRs in our study was 96, about 30 of them at high latitudes. No two ETRs are exactly similar, and features such as orientation, height in the solar atmosphere, visibility, background brightness, etc., also affect the measured values in the radio, CaII(k_3), H_α images and in the magnetograms. Instead of concentrating on individual ETRs, it is therefore more sensible to consider the whole data set in order to find general trends and relations between the various measured properties.The following comparisons were obtained for our set of ETRs:

1. The change in the maximal brightness in CaII(k_3), H_α and maximal values of the magnetic field strength in the magnetograms as a function of the surface area (i.e., within the set of radio ETR contours $\{k_n\}$; see Figs. 6A–C).

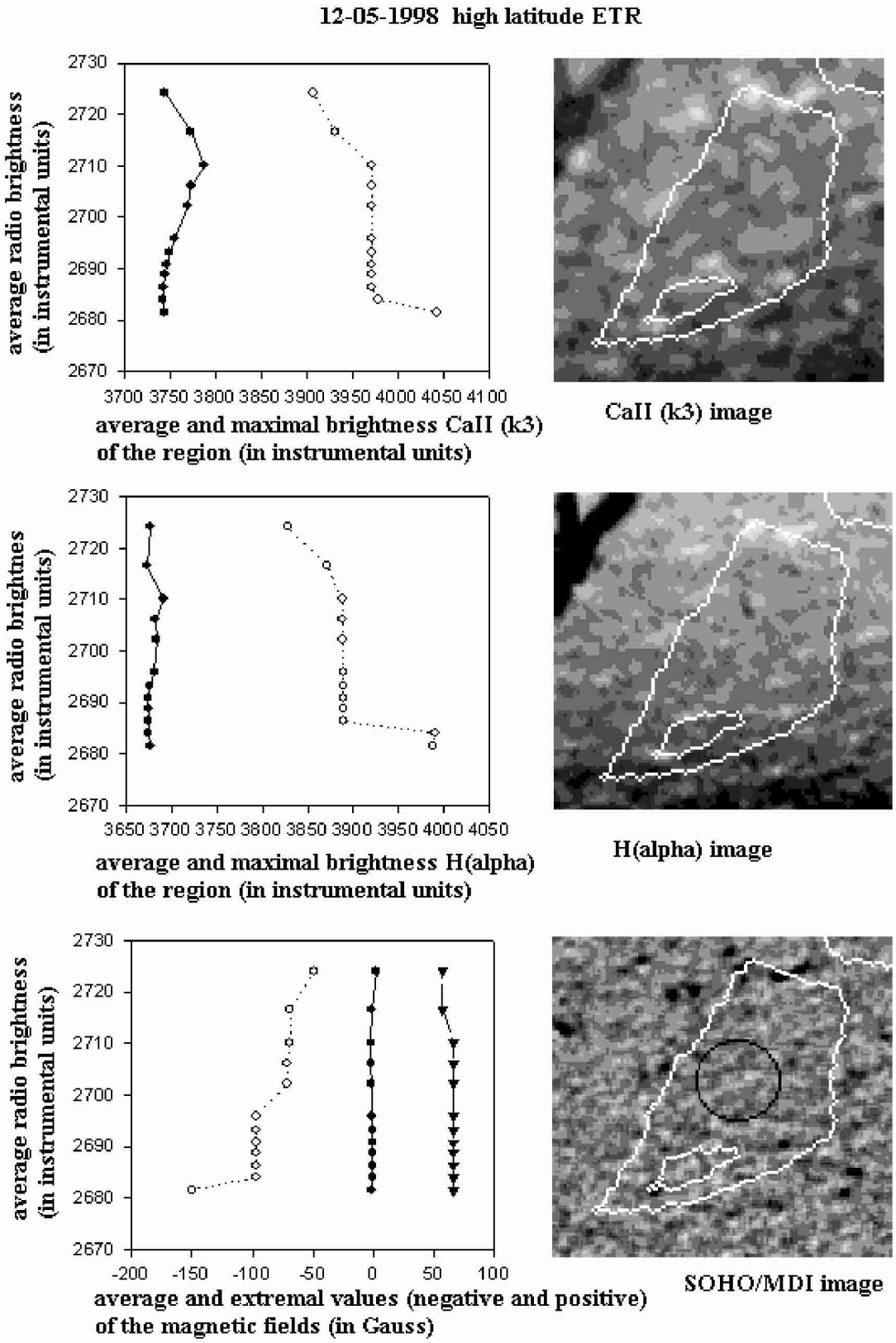

Fig. 4. Details of the CaII(k_3) and H_α intensitygrams and SOHO/MDI magnetograms with superposed radio contours, and relations between the average radio brightness and other wavelength data (see the main text for explanations).

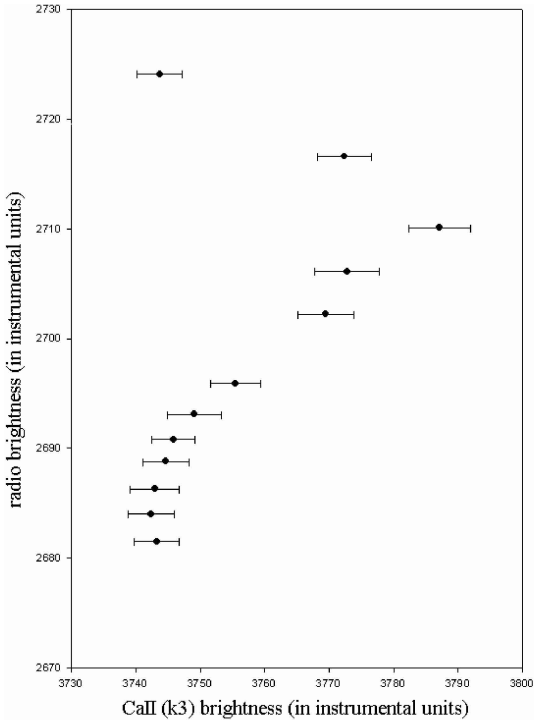

Fig. 5. Relation between the average radio brightness and the average CaII(k_3) brightness (with error bars) for the ETR in Fig. 4.

2. The change in the average surface brightness in radio, CaII(k_3), H_α and in the magnetic field strength, see Figs. 7A–D.

3. The dependence between the average radio brightness and the average CaII(k_3) and H_α brightness; see Figs. 8A, B.

4. The dependence between both the maximal and the average brightnesses in CaII(k_3) and in H_α regions; see Figs. 9A, B.

5. The dependence between the average magnetic field strength and the average radio, CaII(k_3) and H_α brightness; see Figs. 10A–C.

6. The dependence between the maximal magnetic field strengths and the maximal CaII(k_3) and H_α brightness; see Figs. 11A, A1, B and B1.

4.1. Location of the ETR maximum relative to the surface maximal brightness features and maximal magnetic field strength sources

The Metsähovi radio telescope beam has a size of about 1000 msh (millionths of the solar hemisphere) in the center of the solar disk, and approximately 2000 msh at a relative distance of $r/R = 0.9$ from the center. This sets a limit to the positional accuracy with which we can compare radio to the other data. When we look at relations within the innermost contour region around the ETR maximum, i.e. surface areas between 0 and 2000 msh, we cannot any longer be certain to what extent the changes are due to positional mismatches between the radio and the other wavelengths.

Figure 6A shows how the maximal brightness in the CaII(k_3) regions changes with the ETR surface area as we zoom in from the outermost ETR contour towards the ETR maximum at $S = 0$ msh. Each curve corresponds to one region. If the CaII(k_3) maximum coincides with the radio maximum, each curve should be a straight horizontal line (with a possible drop of in the $S = (0{-}2000)$ msh region due to the positional mismatch discussed above). We can see that this is indeed the case for the majority of the ETRs: each contains a CaII(k_3) region with a maximal brightness between 5 and 20 percent above the disk average; within the observational accuracy this "local brightest feature" (i.e., the brightest CaII feature within the radio ETR) also coincides with the radio maximum.

There are also ETRs in which the local brightest CaII feature clearly is situated outside the contour corresponding to the $S = 2000$ msh area. In these regions the radio and the CaII maxima do not coincide, and the maximal CaII brightness decreases as we close into the radio maximum. However, in the radio maximum area ($S < 2000$ msh) these regions still contain "minor brightness features" which, even if dimmer than the local brightest feature, still have intensities at or above 1.02 in normalized units.

Thus we can conclude that there seem to be two different types of behaviour:

1. Regions in which the radio maximum position coincides with the local brightest CaII feature.

2. Regions in which the radio maximum position is offset from the local brightest CaII feature, but coincides instead with minor brightness features above the average CaII surface brightness level.

Almost all the mentioned above conclusions are valid also for the maximal brightness of the H_α regions (see Fig. 6B). When the radio maximum is offset from the local brightest H_α feature (the second type of behaviour), it in some cases seems to coincide with a H_α minor brightness feature hardly above the average background level.

Figures 6C and C1 show how the maximal magnetic field strength changes with the ETR surface area. The typical collective behaviour of the magnetic features is very similar to the two previous cases. As in the previous cases, we can see the magnetic field structures (straight horizontal lines with a possible falling of in the $S = (0{-}2000)$ msh region due to positional mismatch), which coincide with the nominal maxima of the ETRs. There are also ETRs which do not seem to coincide with discernible magnetic field strength increases. In almost all cases the maximal magnetic field strengths in the vicinity of the nominal maxima of the ETRs are larger than 40 Gauss, but less than 500 Gauss.

4.2. The average surface brightness and magnetic field strength in the ETR regions

In the previous section we have found out that the brightest CaII(k_3) and H_α features, as well as the strongest magnetic features within the ETRs, often coincide with the radio maxima. However, within the enhanced temperature regions there are both bright and dark features, as can be seen in Fig. 4. In this section we therefore study whether the *average* surface brightness within the ETR contours $\{k_n\}$ in general is larger than the

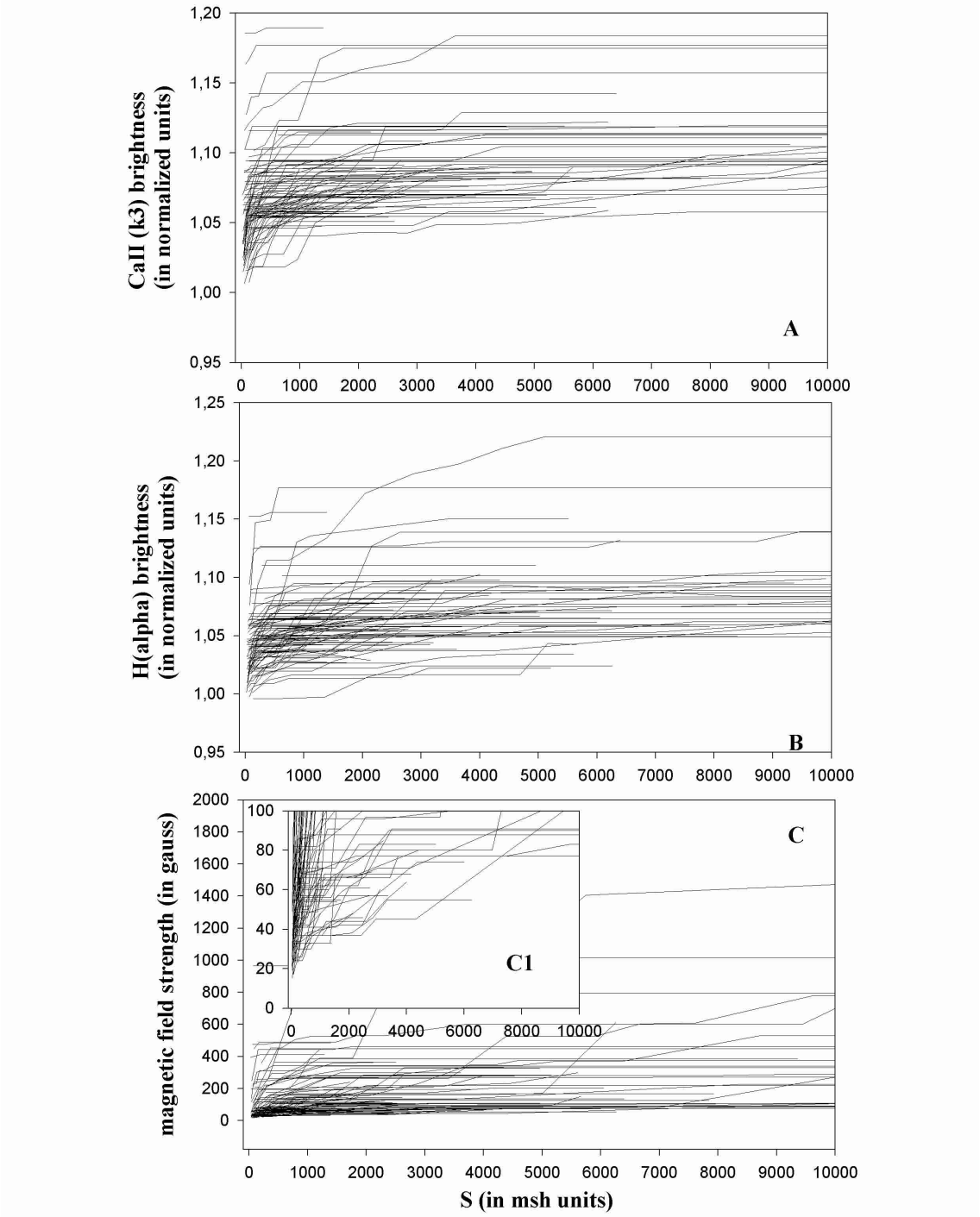

Fig. 6. The change in the maximal brightness and the maximal magnetic field strength as a function of the ETR intensity contour or area. **A)**: CaII, **B)**: H_α, **C)**: SOHO/MDI magnetic field strength, **C1)**: enlargement of **C)** in the magnetic field strength interval from 0 to 100 Gauss.

solar disk average, and how it relates to the radio data. In each case, the average brightness was found by summing together the fluxes in the individual pixels within a given ETR contour and dividing it by the number of pixels in the area bounded by the contour.

Figure 7A shows the variation of the average surface radio brightness ($\{r_{avn}\}$) with the ETR area. All curves naturally show a monotonic increase as the area is decreased around the ETR maximum. The two highest values, shown for comparison, correspond to ETRs associated with sunspot activity.

Figure 7B shows the change in $\{Ca_{avn}\}$. We can see that almost all regions have an average brightness larger than 1.0 (the "quiet Sun level" in the CaII(k_3) solar images). Usually, there is also a slight monotonic increase as the ETR area decreases from 10 000 msh to 2000 msh. When the area is smaller than 2000 msh, $\{Ca_{avn}\}$ either increases more rapidly

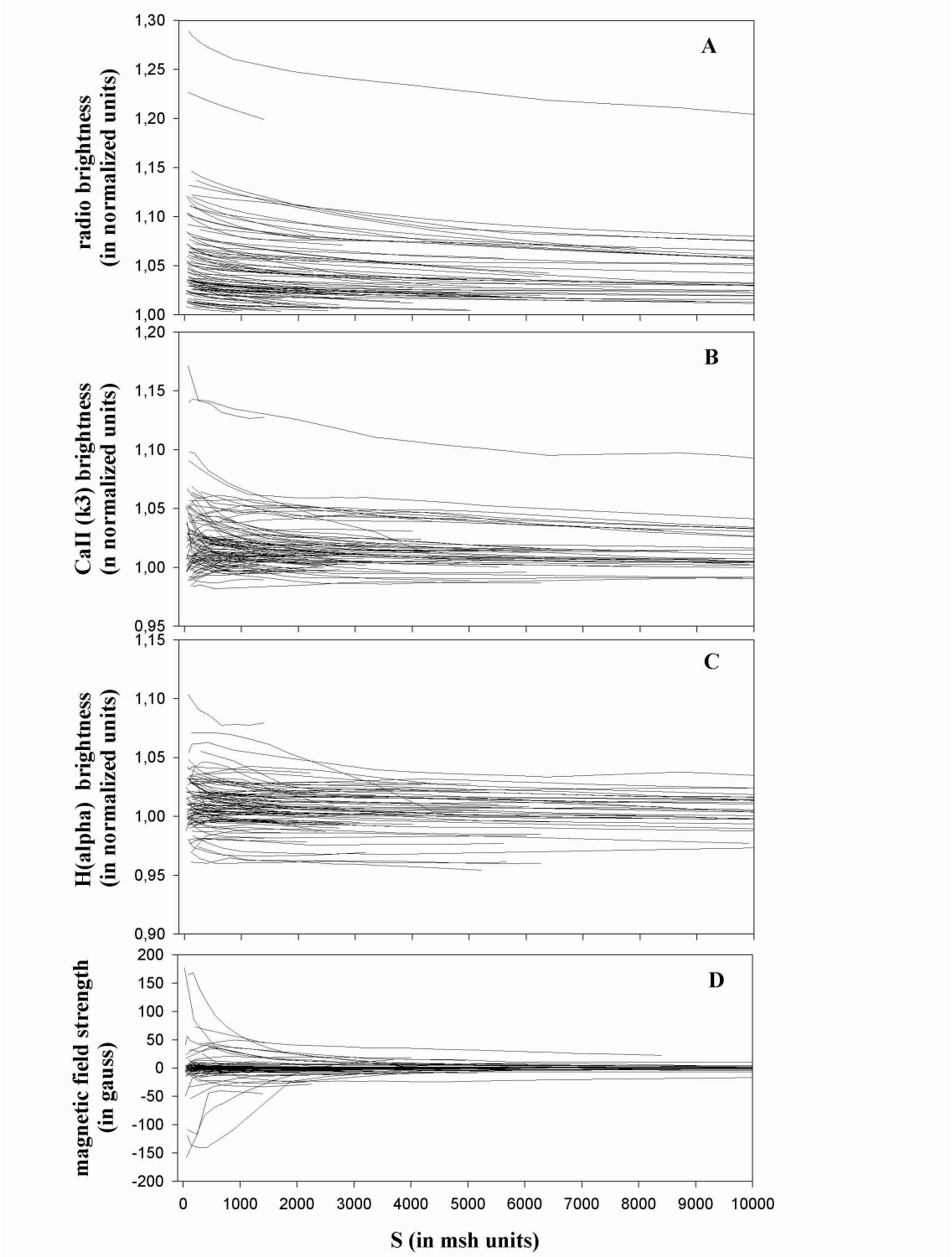

Fig. 7. The change in the average brightness and the average magnetic field strength as a function of the ETR intensity contour area. **A)**: radio, **B)**: CaII, **C)**: H_α, **D)**: SOHO/MDI magnetic field strength.

or decreases, again depending on whether the nominal ETR maximum position coincides with the local brightest feature or not. Again, the two highest values correspond to sunspot activity.

Figure 7C shows the change in $\{H_{avn}\}$. In principle, it looks quite similar to the CaII(k_3) case. However, although the average of the whole data set is slightly above the H_α quiet Sun level, a considerable number of ETR regions correspond to areas with $\{H_{avn}\}$ below 1.0.

Figure 7D shows the change in $\{m_{avn}\}$ in the same regions. For most regions, $\{m_{avn}\}$ remains close to zero, but some regions exhibit considerable changes in the area interval from $S = 2000$ msh to $S = 0$ msh. This is probably connected with the symmetric or non-symmetric disposition of the radio

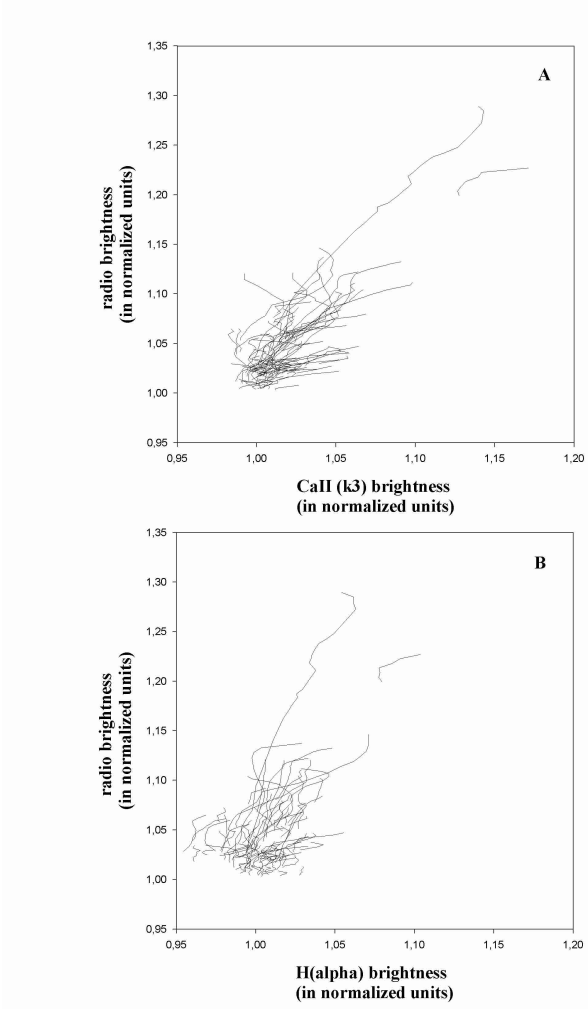

Fig. 8. Relations between the changes in the average surface brightness of radio, CaII(k_3) and H_α regions. The two highest intensities are from sunspot regions, selected for comparison.

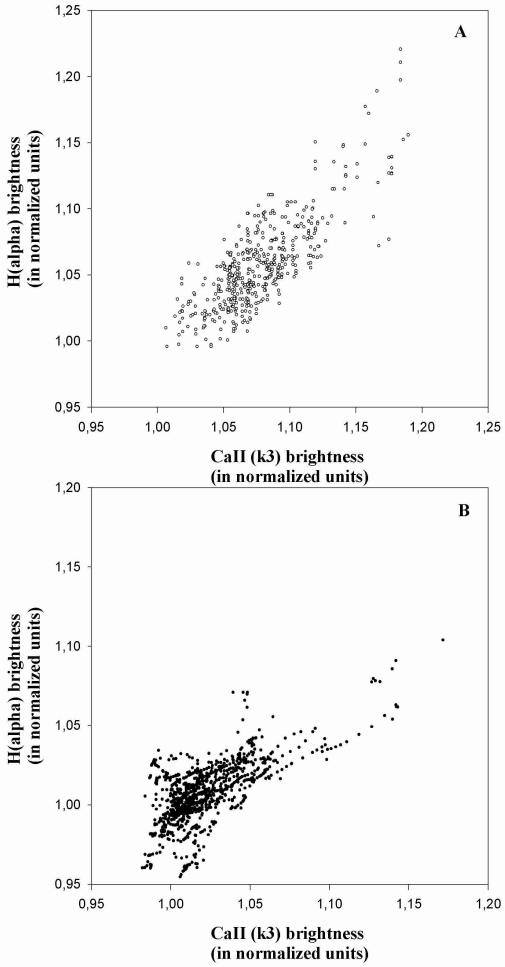

Fig. 9. The correlation between the maximal **A)** and the average **B)** CaII(k_3) and H_α brightnesses in the enhanced radio temperature regions.

maxima relative to the magnetic field sources in areas small enough to see this effect. On the other hand, it also indicates that there are magnetic field structures close to the radio maximum positions.

4.3. The correlation between the average radio brightness and the average CaII(k_3) and H_α brightness

Figures 8A and B show a comparison between the average radio brightness and the CaII(k_3) and H_α brightness. Each curve corresponds to a single ETR. For clarity, we have joined the individual measurements corresponding to the areas bounded by $\{k_n\}$ in each ETR. The two sunspot ETRs are again readily apparent by their high brightness as compared to the weak ETRs.

Considering the data set as a whole, we can see that $\{r_{\mathrm{avn}}\}$ correlates both with $\{Ca_{\mathrm{avn}}\}$ and with $\{H_{\mathrm{avn}}\}$, except for the smallest brightness enhancements. The dependence is in general almost linear, as is also the case for the whole data set. However, for individual regions the dependence shows considerable variation.

It should be remembered that we have studied only the areas defined by the radio enhanced temperature regions. These correlations are therefore valid only within the ETRs and do not, for example, imply a general correlation between the radio and the $\{Ca_{\mathrm{avn}}\}$ brightness over the solar surface.

4.4. Correlations between the maximal and the average CaII(k_3) and H_α brightness

The maximal brightnesses of the CaII and the H_α are quite well correlated, with almost linear dependence as shown in Fig. 9A. This means that within the ETRs we see the same "local brightest" features in the different spectral lines.

Average CaII(k_3) and H_α brightnesses are related to each other, too (see Fig. 9b). However, there is a relatively large scatter especially with weak enhancements, when $\{Ca_{\mathrm{avn}}\}$ and $\{H_{\mathrm{avn}}\}$ have values around 1.0. Again, these correlations are valid only within the ETRs, as in the previous section.

4.5. Relations between the average magnetic field and $\{r_{avn}\}$, $\{Ca_{avn}\}$ and $\{H_{avn}\}$

These relations are shown in Figs. 10A–C. In general, these relations look similar. One can see that there are many regions with enhanced $\{r_{\rm avn}\}$, $\{Ca_{\rm avn}\}$ and $\{H_{\rm avn}\}$, but with almost no variation in $\{m_{\rm avn}\}$. The average magnetic field does deviate from the zero level for the highest brightness regions, which in general correspond to the smallest areas ($S = 0-2000$ msh). This is not unexpected, since the likelihood of having just one magnetic pole within a brightness contour naturally increases with decreasing area. However, there are also some larger regions where the average magnetic field deviates from zero (see also Fig. 7D).

4.6. Relations between the maximal CaII and H_α brightness and the maximum magnetic field strength

Relations between the maximal magnetic field strength (at the photospheric level) and the maximal brightness of CaII(k_3) and H_α are shown in Figs. 11A and B, with enlargements of the central parts shown in Figs. 11A1 and B1. One can see that for some regions there is an almost linear dependence between the maximal magnetic field strength and the maximal CaII or H_α brightness in the interval from around 25 Gauss to 100 Gauss. In other regions no connection with the magnetic field strength is apparent, the lack of correlation resulting in almost horizontal lines, in particular for large field values in excess of 150 Gauss. However, these relatively strong magnetic field strengths could still be a necessary prerequisite for the existence of the bright structures.

Thus we can conclude that there are both "magnetic" and "non-magnetic" brightness features in the radio enhanced temperature regions. This is in agreement with the results obtained by Nindos & Zirin (1998) for the relation between the intensity of CaII(K)-line bright features and the intensity of the associated magnetic elements.

5. Discussion

The radio ETRs, at both high and low latitudes, are clearly connected to brightness structures seen in the CaII(k_3) and H_α images. In general, after superposing the ETR radio contours on the CaII(k_3) and H_α images, we find that most radio-enhanced regions are enhanced in CaII(k_3) and H_α brightness also. This effect is clearer in CaII than in H_α. The largest radio enhancements correspond to sunspot complexes, a few of which were included in this study for comparison purposes.

All three average brightnesses correlate with each other in an approximately linear manner. If we look at the whole data set, the brightest CaII and H_α structures also tend to have stronger magnetic fields (see Fig. 11), but a dependence between the brightness and the maximal field strength is found in only a fraction of the individual regions, most of them rather weak.

The situation is less clear for the maximal magnetic field strength and the ETR maxima, because our radio map resolution is not sufficient. Using a better radio resolution (10 arcsec as compared to our one arcminute),

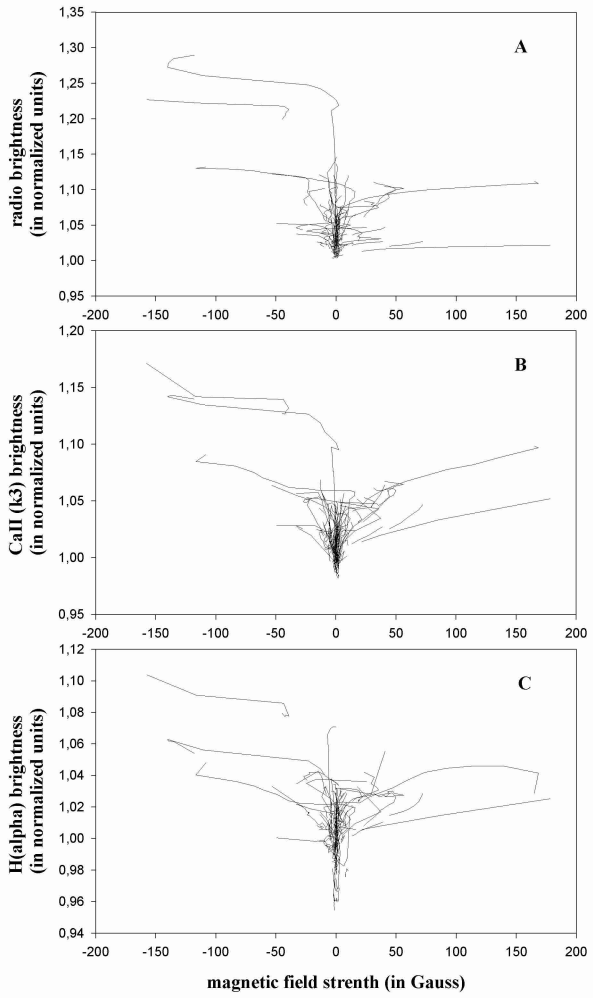

Fig. 10. Relations between the variations of $\{m_{\rm avn}\}$ and $\{r_{\rm avn}\}$ **A)**; $\{Ca_{\rm avn}\}$ **B)**; $\{H_{\rm avn}\}$ **C)**.

Gopalswamy et al. (1999) found a clear spatial connection between the coronal hole radio brightenings and photospheric magnetic field structures. Our results provide only indirect support for this result, because it was impossible to compare the positions of the magnetic field structures and the true radio maxima. However, we find a relation between maximal magnetic field structures and maximal brightness CaII/H_α structures. On the other hand, all these brightness structures are related to the radio ETRs, as suggested in our study.

We have found that there seem to be two different classes of enhancements. In the first class, the radio maximum coincides with the CaII/H_α maximum and the maximal magnetic field strength structures within the observational accuracy. In this case the average brightness increases monotonically between $S = 10\,000-2000$ msh as the radio contours get closer to the radio ETR maximum, and the maximal values of brightness of CaII/H_α and magnetic field strength remains constant.

In the second class, the radio and the local CaII/H_α/magnetogram maxima are offset from each other. The maximal brightness and magnetic field strength, and possibly also the average brightness, starts to decrease before the contour corresponding to $S = 2000$ msh is reached. In these cases the

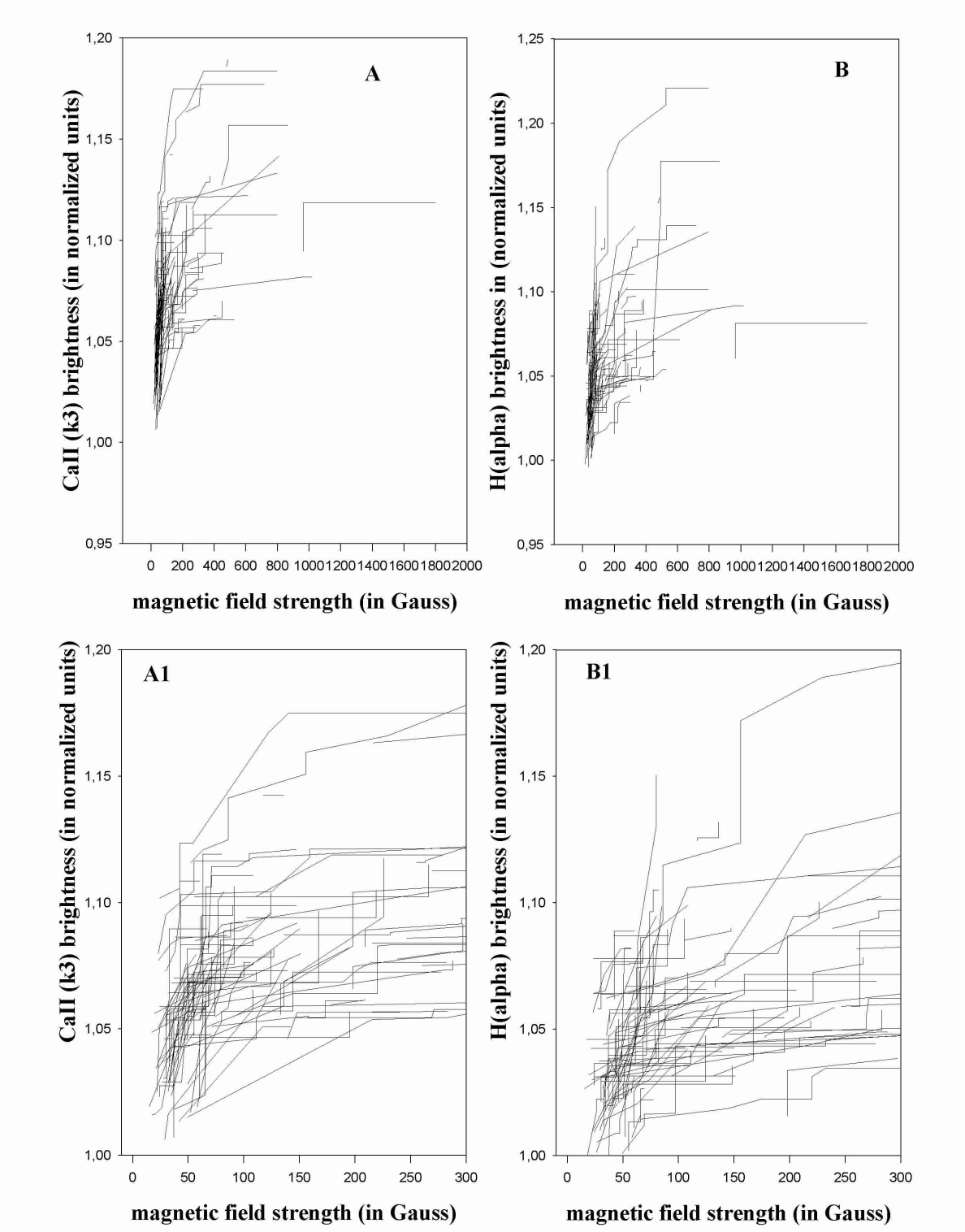

Fig. 11. Relations between the maximal CaII(k_3) **A)** and H_α **B)** brightness features and maximal magnetic field strength structures. Figures **A1)** and **B1)** are enlargements of the central parts of Figs. **A)** and **B)**.

radio maximum corresponds to brightness levels above the disk average but below the maximal values for the whole radio ETR.

The resolution in the radio data, 1 arcmin at 87 GHz, makes it impossible to study the fine structure of the radio enhancements directly. At scales smaller than the projected Metsähovi beam area, $S < 2000$ msh, there could be one single main radio structure responsible for the radio intensity peak. Alternatively, the maximum could be due to the integrated emission from a number of smaller unresolved radio enhancements.

On the basis of the close relations between the weak brightness enhancements, it is possible to speculate that these two alternatives could correspond to the two different classes of ETRs suggested in our study. If there is only one main radio structure responsible for the radio maximum, it coincides with

the CaII/H_α/magnetogram maximum. If there is considerable fine structure in the radio emission, its peak may be offset from the CaII/H_α/magnetogram maximum. In this case, there could, e.g., be an enhancement in the average density of the less intense CaII/H_α brightness features, each also corresponding to a small individual radio ETR. The integrated emission from these unresolved ETRs is then responsible for the observed radio maximum.

It is sometimes assumed that at least a fraction of the radio brightenings are caused by polar coronal holes, since they were initially discovered in the coronal holes and have in later studies often been found to be associated with them. But no one-to-one correlation between radio brightenings and coronal features has been found in previous studies. Other part radio brightenings are associated with the faculae (which often have enhancement in CaII/H_α lines). In the present work we did not consider coronal holes, although from previous work it was known that many of the studied ETRs are located inside coronal holes, in particular at high latitudes (Riehokainen et al. 2001). We cannot therefore know whether the suggested division of ETRs into two different types has any relation to the presence of a coronal hole. In our future work we will consider also the spatial-temporal relationships of the CaII/H_α bright structures with the coronal holes and non-coronal hole areas. We believe that such a study will also improve our understanding of the nature of the radio enhanced temperature regions also.

An interesting fact is that coronal holes rotate rigidly (Wagner 1975; Timothy et al. 1975), while radio ETRs and other photospheric and chromospheric structures exhibit differential rotation (Riehokainen et al. 1998; Gelfreikh et al. 2002a,b). Thus, in general, the coronal holes are in relative motion with respect to the photosphere and the chromosphere. It is therefore possible to suggest a non-causal connection between the coronal holes and the ETRs: the relative motion of the coronal hole brings into view weak structures, which would remain undetectable outside coronal holes, and which can be responsible for the ETRs.

6. Conclusions

In this work we have studied the relations between average and maximal brightness (or magnetic field strength) characteristics in the CaII(k_3), H_α lines and in the magnetograms in areas within radio enhanced temperature regions observed at 87 GHz during five days in 1997, 1998 and 2000. Altogether 96 low and high latitude ETRs were included in the study, most of them quite weak in comparison with the well-known strong ETRs associated with sunspots. The comparisons were made by measuring both the average and the maximal brightness (in the magnetic field case, the greatest field strength values) within each radio ETR intensity contour. In this way we could study the positional coincidences between the radio enhancements and the average/maximal brightness (or magnetic field) enhancements, as well as investigate whether there are relations between their strengths.

We found that, almost without exception, the average CaII brightness of a radio ETR is higher than the disk average. The average H_α brightness is also larger in most ETRs. However, the relative brightness enhancement is smaller than for CaII, and there are more cases where the average H_α brightness is comparable to, or even below, the disk average. Only a few radio ETRs have non-zero average magnetic field strength.

There is also a clear positive correlation between the relative average brightness of the radio, CaII and the H_α. Within each successive radio intensity contour closer to the radio maximum, the average CaII and H_α brightness also tends to increase. In most cases there is no change in the average magnetic field strength.

In most cases the brightest local CaII, H_α features (i.e., the brightest feature within the area defined by the outermost radio ETR intensity contours) and maximal magnetic field structures appear to coincide with the radio maximum. The observational accuracy of this positional coincidence is limited to $S \approx 2000$ msh by the projected size of the radio telescope beam. However, there are also a number of regions in which the CaII, H_α and magnetogram local maxima are clearly offset from the radio maximum. In these regions the radio maximum coincides with minor CaII, H_α brightness and magnetic field enhancements, smaller than the local maxima but still above the disk average. The local magnetic field maxima are larger than 40 Gauss. There thus seem to be two different classes of weak ETRs with different fine structures. Further investigations will require better radio resolution. The possible connection to the the presence of a coronal hole also need, to be investigated. In the present analysis no distinction was made between radio ETRs inside and ouside of coronal holes.

Finally, we could not find any differences between weak high latitude and weak low latitude ETRs. They therefore appear to have similar physical causes.

References

Babin, A. N., Gopasyuk, S. I., & Efanov, V. A. 1976, Izv. Krymsk. Astrfiz. Obs., 55, 3

Efanov, V. A., Labrum, N., & Moiseev, I. G. 1980, Izv. Krymsk. Astrfiz. Obs., 61, 52

Gelfreikh, G. B., Makarov, V. I., Tlatov, A. G., Riehokainen, A., & Shibasaki, K. 2002a, A&A, 389, 618, Paper I

Gelfreikh, G. B., Makarov, V. I., Tlatov, A. G., Riehokainen, A., & Shibasaki, K. 2002b, A&A, 389, 624, Paper II

Gopalswamy, N., Schmal, E. J., & Kundu, M. R. 1992, Proc. First SOHO Workshop, Coronal Streamers, Coronal Loops and Coronal and Solar Wind Composition, 113

Gopalswamy, N., Shibasaki, K., Thompson, B. J., Gurman, J., & DeForest, C. 1999, JGR, 104

Kosugi, T., Ishigiro, M., & Shibasaki, K. 1986, Publ. Astron. Soc. Jpn., 38, 1

Moran, T., Gopalswamy, N., Dammasch, I. E., & Wilhelm, K. 2001, A&A, 378, 1037

Nindos, A., & Zirin, H. 1998, Sol. Phys., 179, 253

Pohjolainen, S., Portier-Fozzani, F., & Ragaigne, D. 2000, A&A, 143, 227

Riehokainen, A., Urpo, S., & Valtaoja, E. 1998, A&A, 333, 741

Riehokainen, A., Urpo, S., Valtaoja, E., et al. 2001, A&A, 366, 676

Shibasaki, K. 1997, Synoptic Solar Physics, ed. K. S. Balasubramaniam, J. Harvey, & D. Rabin, ASP Conf. Ser., 140, 373

Timothy, A. F., Krieger, A. S., & Vaiana, G. S. 1975, Sol. Phys., 42, 135

Vernazza, J. E., Avrett, E. H., Loeser, R. 1981, ApJS, 45, 635

Wagner, W. 1975, ApJ, 198, L141